



Assessing the effect of land cover on ISBA snow water equivalent simulations over Europe

5 Oscar Rojas-Munoz¹, Constantin Ardilouze¹, Bertrand Bonan¹, Diane Tzanos¹, Darren Ghent², Céline Lamarche³, Thomas Nagler⁴, and Jean-Christophe Calvet¹

¹Météo-France, CNRS, Univ. Toulouse, CNRM, Toulouse, France

²National Centre for Earth Observation, Department of Physics and Astronomy, Univ. Leicester, Leicester, UK

³Earth and Life Institute, Environmental Sciences, Univ. catholique de Louvain, Louvain-la-Neuve, Belgium

⁴ENVEO IT GmbH, Innsbruck, Austria

10

Correspondence to: Jean-Christophe Calvet (jean-christophe.calvet@meteo.fr)

Abstract. An accurate representation of the land surface is essential for simulating the exchange of energy, water and carbon between the land and the atmosphere. This study evaluates the impact of land cover representation on snow simulations in the Interactions Between Soil, Biosphere and Atmosphere (ISBA) land surface model in Europe between 2010 and 2022.

15 The study employs the European Centre for Medium-Range Weather Forecasts (ECMWF) ERA5 atmospheric forcing dataset. Offline simulation experiments were conducted using two different versions of the model to prescribe land cover. The most recent version uses the latest land cover data from the European Space Agency's (ESA) Climate Change Initiative (CCI). The model's ability to reproduce snow dynamics was evaluated through a comparison of the simulations with ESA CCI satellite snow water equivalent (SWE) retrievals and ERA5 snow analyses. The ERA5 analysis shows the highest level 20 of agreement with satellite observations of SWE at the domain scale. On average, both the ERA5 and ISBA simulations tend to overestimate SWE compared to the CCI SWE. However, it is also possible that the CCI SWE product underestimates the actual SWE. This bias is particularly large during the warm winter of 2020, while the scaled SWE anomalies are comparable to those observed by ESA CCI and ERA5. Using ESA CCI land cover data reduces the ISBA SWE bias by around 33%, with this reduction being observed over most of the domain. These findings emphasise the importance of accurate land cover 25 data for improving snow representation in land surface models and highlight the need for updated vegetation information in future snow-related applications.

1 Introduction

Land surface models (LSMs) are essential for simulating energy, water and carbon fluxes at the interface between the land and the atmosphere. They are widely used in weather forecasting, climate modelling and hydrological applications, such as 30 predicting droughts and floods (Crow et al., 2012; Mishra et al., 2024; Quintana-Seguí et al., 2020), as well as informing land-use and water-use policy (Blyth et al., 2021). However, the accuracy of LSM outputs depends heavily on the quality of boundary conditions and surface parameters, particularly land cover (LC) data. LC maps are used to define key properties



such as albedo, roughness, rooting depth and vegetation type. These properties modulate surface fluxes and soil–vegetation–atmosphere interactions (Bounoua et al., 2002; Levis, 2010). Traditional LC datasets used in LSMs often rely on static or 35 outdated classifications that may no longer accurately reflect current land use patterns or vegetation changes caused by climate change and human activity (Maas et al., 2018). Updating these datasets is important in order to better estimate surface heat fluxes and soil temperature (José et al., 2024). ECOCLIMAP-II (Faroux et al., 2013), for example, has long been the reference within the SURFEX modelling system (Masson et al., 2013), providing global 1 km resolution maps. Over Europe, ECOCLIMAP-II is based on data from the early 2000s (Kaptue et al., 2009; Etchanchu et al., 2017). However, 40 it does not incorporate recent satellite-derived LC changes. To overcome these limitations, a new LC product called ECOCLIMAP-SG (Calvet and Champeaux, 2020) has been developed. This product integrates LC data from the European Space Agency (ESA) Climate Change Initiative (CCI) LC v2.0.7 product with vegetation data from the Copernicus Land Monitoring Service (CLMS). This fusion enables the representation of LC changes at a resolution of 300 metres and incorporates inter-annual LC variability and seasonal vegetation dynamics (Barella-Ortiz et al., 2022; Li et al., 2018). 45 Previous research has shown that dynamic, high-resolution LC data can enhance the modelling of vegetation growth, energy flux partitioning, albedo, and hydrological processes (Lawrence & Chase, 2007; Liu et al., 2021; Wang et al., 2023). Although improvements to LC datasets can reduce uncertainties in surface parameterisation, it is still important to validate these updates against independent observations. Satellite-based Earth observation (EO) products provide a valuable way of assessing the accuracy of model outputs over large areas and long periods of time. Recent advances in EO have enabled the 50 development of long-term, harmonised satellite products (Gao et al., 2013; de Jeu et al., 2008), which are crucial for validating and benchmarking LSMs. Notably, the ESA Climate Change Initiative (CCI) has produced global datasets for critical surface variables, including snow water equivalent (CCI SWE) and land surface temperature (CCI LST). The CCI products are derived from multi-sensor satellite observations using consistent retrieval algorithms, and have been validated against ground-based measurements to ensure reliability across various climate regimes (Sun et al., 2025; Ling et al., 2021; 55 Pérez-Planells et al., 2023; Reiners et al., 2021; Saeedi et al., 2021). Their spatial resolution and temporal coverage make them suitable for evaluating models at regional to continental scales, helping to identify biases in models and assess structural or parametric deficiencies (Raoult et al., 2018; Seo and Dirmeyer, 2022).

This study evaluates the impact of integrating updated LC information into the Interactions Between Soil, Biosphere and Atmosphere (ISBA) LSM, by benchmarking simulations driven by old LC data and updated CCI LC data. The aim is to 60 assess the influence of the updated LC dataset on the simulation of SWE. We use ESA CCI satellite products and the European Centre for Medium-Range Weather Forecasts (ECMWF) ERA5 reanalysis (Kouri et al., 2023) as reference datasets to evaluate model performance. .

This study is organised as follows: Section 2 presents the model configuration and observational datasets. Section 3 describes the experimental design. Section 4 presents the benchmarking results. Section 5 discusses the findings of this 65 study. Finally, Section 6 outlines future research directions and provides conclusions.



2 Model and data

2.1 ISBA model

The ISBA land surface model is integrated within the SURFEX modelling framework, which was developed by the Centre National de Recherches Météorologiques (CNRM) (Masson et al., 2013). Its purpose is to simulate the exchange of energy,

70 water and carbon between snow, the soil-plant system, and the atmosphere. ISBA operates in both coupled and offline modes and is used for a variety of applications, ranging from operational weather forecasting (Giard and Bazile, 2000; Bélair et al., 2003a,b) to climate simulations (Delire et al., 2020). The ISBA model computes various land surface variables, such as soil moisture and temperature, as well as heat, water and energy fluxes. The model can operate at different timescales, ranging from hours to days, and at different spatial scales, ranging from local to global.

75 This study uses SURFEX version 9 (CNRM, 2023) in offline mode over Europe, i.e. without interacting with an atmospheric model. The configuration used here to represent the soil-plant system is ISBA-A-gs, which is CO₂-responsive and explicitly simulates carbon fluxes, gross primary production, and vegetation growth by resolving leaf-level photosynthesis and stomatal conductance (gs) processes (Calvet et al., 1998, 2008). This configuration dynamically computes leaf biomass and leaf area index (LAI) through balancing net carbon assimilation (A) and photosynthesis-dependent senescence using plant 80 functional type-specific SLA (Specific Leaf Area).

Snow is represented using a medium-complexity snow physics scheme called ISBA-ES (Explicit Snow), which was developed by Boone and Etchevers (2001) and updated by Decharme et al. (2016). The vertical evolution of soil temperature and moisture is computed using a multi-layer diffusion scheme (Boone et al., 2000; Decharme et al., 2019). In this study, snow is represented with twelve layers and the soil is divided into up to 14 layers, with a maximum depth of 12 metres for 85 temperature and 2 metres for moisture, depending on the characteristics of the vegetation. Simulations of snow water equivalent (SWE) and land surface temperature (LST) are analysed.

2.2 CCI SWE data

As part of the ESA CCI, the CCI Snow project provides a long-term, consistent and well-calibrated climate data record of snow water equivalent (SWE) for the Northern Hemisphere (Luoju et al., 2024). This record is derived from passive 90 microwave radiometer observations during the winter season (October to May). The SWE product (version 3.1) spans the period from January 1979 to May 2022, offering daily coverage at a spatial resolution of 0.10°. It is based on measurements from the SMMR, SSM/I and SSMIS sensors aboard the Nimbus-7 and DMSP platforms. The retrieval algorithm uses the GlobSnow methodology (Luoju et al., 2021) to combine satellite microwave observations with in situ snow depth data via a Bayesian assimilation scheme. This enables robust SWE estimates to be generated, masked for mountainous, glaciated, and 95 coastal regions where retrievals are less reliable. In this study, the daily SWE product from the CCI Snow project is regridded to a coarser resolution of 0.25° to match the horizontal resolution of the ISBA land surface model outputs. The focus is on the European domain, where SWE from satellite observations is compared with ISBA-simulated SWE under two



different land cover configurations. The aim is to evaluate the effect of updating the land cover map on modelled snow mass, and to assess the spatial and seasonal consistency of modelled and observed SWE patterns. Given its multi-decade consistency and independence from the ISBA model inputs, the CCI SWE product provides a reference for evaluating the influence of vegetation representation on snow simulations.

2.3 ERA5 SWE data

In this study, we include SWE data from the ERA5 reanalysis in order to provide an additional, model-based reference with which to compare ISBA simulations and satellite observations. ERA5 is the fifth generation of ECMWF atmospheric reanalyses and offers a consistent, physically constrained representation of atmospheric and surface variables globally (Hersbach et al., 2020). The SWE variable takes into account both new snowfall and snow metamorphosis processes. It is computed using a multi-layer snow scheme within the Integrated Forecasting System (IFS), which models processes such as snow compaction, melting and sublimation. Since 2004, ERA5 has assimilated the Interactive Multi-sensor Snow and Ice Mapping System (IMS) product at altitudes below 1500 m. The IMS (Chiu et al., 2020; Orsolini et al., 2019) is produced by the National Oceanic and Atmospheric Administration (NOAA). It combines microwave, visible, and infrared satellite data to produce snow cover data for the Northern Hemisphere with a spatial resolution of 4 km. ERA5 snow depth data is available with an hourly temporal resolution and a horizontal resolution of approximately 31 km, globally, since 1979. In our study, daily averages of snow depth are extracted and interpolated onto the same 0.25° grid as the ISBA outputs over the European domain. Although not an observational product, ERA5 provides a valuable, physically consistent estimate of snowpack evolution that can contextualise differences between model simulations and satellite retrievals.

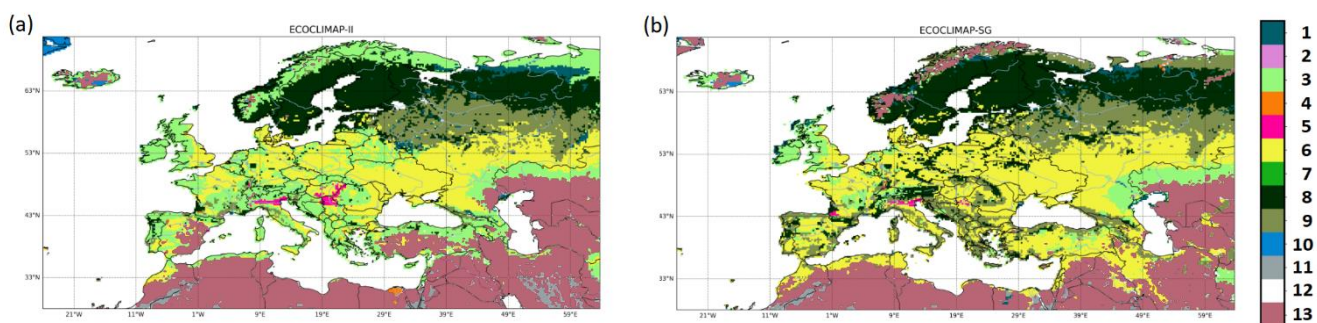
2.4 CCI LST data

The land surface temperature (LST) data used in this study originate from the ESA CCI LST project, which produces various products from different sensors (Pérez-Planells et al., 2023). Thanks to its validated accuracy and temporal consistency, the high-resolution product derived from NASA's Moderate Resolution Imaging Spectroradiometer (MODIS) observations is widely used in climate studies and land surface modelling. The MODIS LST data are available for daytime and night-time overpasses, enabling the characterisation of the diurnal surface temperature cycle across different land types and climate zones. In this study, we use a pre-release version 4 of the Aqua MODIS CCI LST dataset, which is more recent and has been processed at a resolution of 0.05° . This version provides consistent daily LST estimates corresponding to satellite overpass times of approximately 13:30 and 01:30 local solar time (LT), based on Aqua MODIS observations. This temporal resolution allows day and night surface temperature dynamics to be separated. The LST CCI product has been resampled to a resolution of 0.25° .



2.5 CCI LC data

This study investigates the impact of incorporating ESA CCI Land Cover (LC) data into the ISBA land surface model. Two datasets are considered: ECOCLIMAP-II (Faroux et al., 2013) and the updated ECOCLIMAP-SG (Calvet and Champeaux, 130 2020). These LC products are used within the SURFEX platform to define biophysical parameters associated with vegetation types by classifying them into plant functional types (PFTs). These PFTs include categories such as broadleaf and needleleaf forests, C3/C4 crops, irrigated areas, bare soil, grasslands and more. Surface parameters of the ISBA model are associated with each PFT and can vary depending on the local cover composition. For the purposes of this study, a configuration of 12 PFTs has been set. While ECOCLIMAP-II relies on older land cover inventories (Corine Land Cover 2000, GLC2000), 135 ECOCLIMAP-SG integrates higher-resolution ESA CCI LC data at 300 m and accounts for recent land use changes. This study uses LC v2.0.7 for the year 2010. Figure 1 illustrates the dominant land cover types over Europe at a spatial resolution of 0.25°, as represented in ECOCLIMAP-II and ECOCLIMAP-SG. These will be referred to as Old LC and New LC, respectively, throughout the rest of this study.



140

Figure 1: Dominant land cover type over Europe at a spatial resolution of 0.25° x 0.25° as derived from (a) Old LC ECOCLIMAP-II (Faroux et al., 2013), (b) New LC ECOCLIMAP-SG (Calvet and Champeaux, 2020), with CCI LC v2.0.7 2010. The 12 dominants land cover types are indicated in the colour bar: 1 - flooded shrubs or grass, 2 - tropical grasslands, 3 - temperate grasslands, 4 - flooded trees, 5 - C4 crops (e.g. maize), 6 - C3 crops (e.g. wheat), 7 - broadleaf evergreen trees, 8 - coniferous trees, 9 - deciduous broadleaf trees, 10 - permanent snow and ice, 11 -rocks, urban, 12 – ocean and water bodies, 13 – bare soil with no vegetation.

Substantial regional differences emerge due to variations in the source data and methodology. The Old LC tends to underestimate forest cover, particularly coniferous forests, across northern Europe. These forests are more extensively 150 represented in New LC. In contrast, New LC, which integrates more recent, higher-resolution, satellite-derived vegetation products, exhibits finer spatial variability and improved delineation of agricultural and wetland areas. Notably, C4 crops are more accurately localised in southern and Eastern Europe in New LC. There is less bare soil in Mediterranean regions and the Middle East. Irrigation is no longer categorised as a land surface type. Instead, it relies on independent irrigation maps, meaning that all vegetation types can be irrigated (Druel et al., 2022).



155 3 Experimental setup and model evaluation

Two offline experiments were conducted using the SURFEX v9 framework over the European domain (28.125°N–71.875°N, 25.875°W–63.875°E) to evaluate the sensitivity of the ISBA simulations to land cover input. The experiments used Old LC and New LC data. These offline simulations cover the period from January 2010 to September 2022 and are not coupled with an atmospheric model. Instead, they are driven by hourly ERA5 atmospheric reanalysis data (Muñoz-Sabater et al., 2021), which has been interpolated to the ISBA grid at a resolution of $0.25^\circ \times 0.25^\circ$ using bilinear interpolation. LAI and SWE are calculated interactively and are not constrained by satellite observations. Both LC simulations use the ISBA-A-ags and ISBA-ES configurations and have the same model structure and physical parameterisations. To ensure equilibrium of deep soil temperature and root-zone moisture, long spin-up integrations preceded both setups. Specifically, a generic spin-up lasting 200 years was followed by a specific spin-up for Old LC and New LC. The 1981–1989 and 2010–2019 simulations were repeated four times for each, in line with the recommendations of Liu et al. (2025). This ensures stable initial conditions for the evaluation period. The model's outputs are updated every three hours (00:00 UTC, 03:00 UTC, 06:00 UTC and so on) for land grid cells excluding large water bodies, rocks and urban surfaces. The number of valid land grid cells ranges from 34,801 for the Old LC to 35,775 for New LC. These outputs are then compared with satellite observations of snow water equivalent (SWE) and land surface temperature (LST) from the ESA CCI datasets. The ISBA SWE simulations are also compared with ERA5 SWE simulations. We conduct two distinct analyses to benchmark ISBA-simulated skin temperature against LST observations: one for daytime (12:00 UTC) and one for night-time (00:00 UTC), over a subdomain that covers the westernmost part of the domain (10°W–30°E, 28.125°N–71.875°N). This separation improves the assessment of model performance in capturing diurnal temperature variations, which are essential for energy balance and hydrological modelling. This enables us to benchmark the model's performance and quantify the impact of land cover updates. We consider the Pearson correlation coefficient (R), the root-mean square difference (RMSD) and the unbiased RMSD (ubRMSD) score values, together with the mean bias (MB). The square of the RMSD value is equal to the sum of the squares of the ubRMSD and the MB.

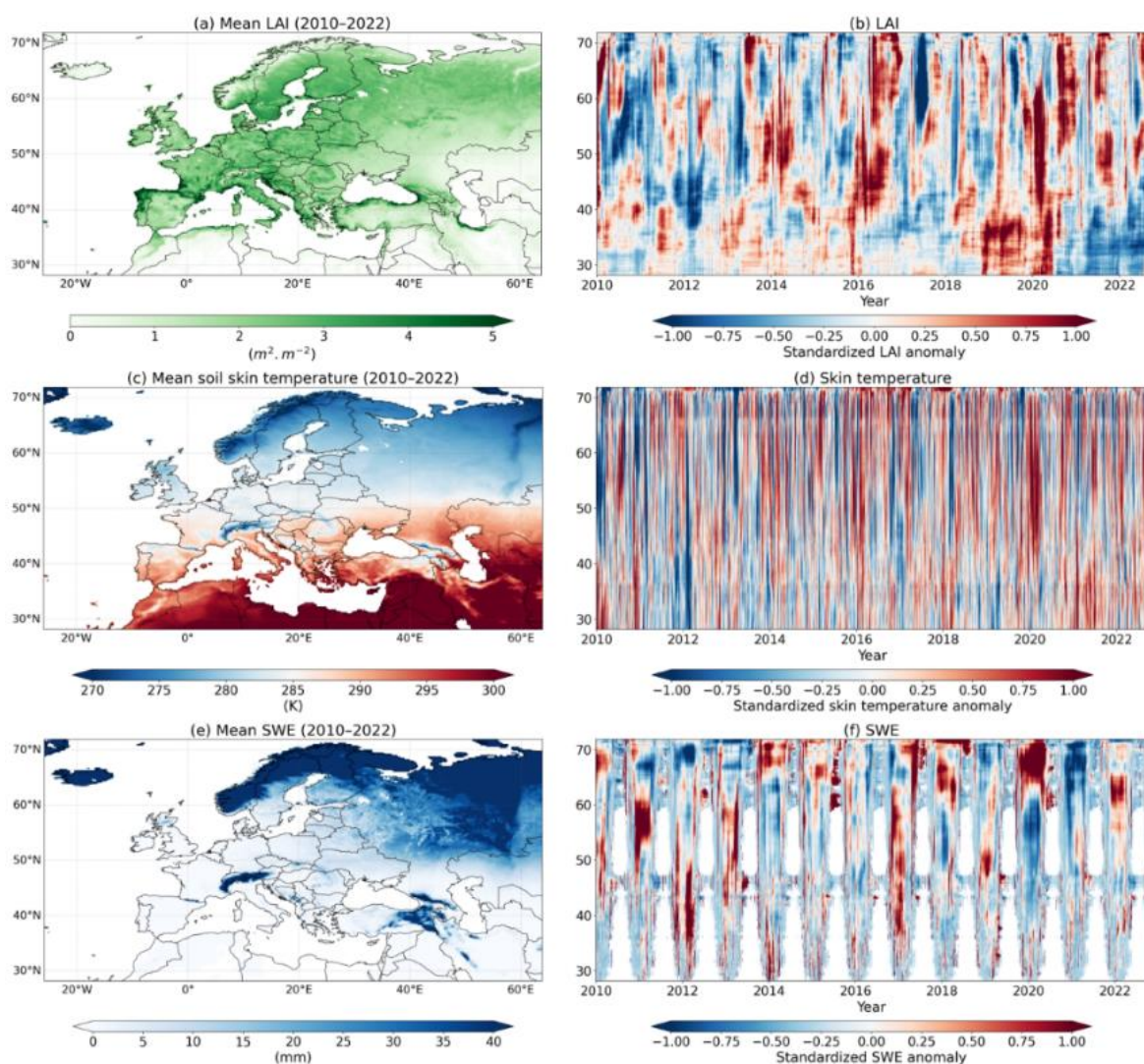
4 Results

4.1 Climatological features and anomaly patterns in ISBA simulations

180 The results of New LC are presented in Figure 2, with a focus on key surface variables: LAI, LST, and SWE. Panels (a), (c) and (e) show the climatological means of LAI, LST and SWE over Europe for the period 2010–2022, respectively. LAI (panel a) is higher in forested areas. LST (panel c) follows latitudinal climatic forcing patterns, with higher values in southern Europe and progressively cooler conditions towards the north. SWE (panel e) is largely confined to northern latitudes and alpine regions, consistent with colder conditions and zones of seasonal snow accumulation. These spatial distributions highlight the expected climate-driven gradients and confirm the physical consistency between surface water,



energy and vegetation processes as modelled in ISBA. The standardised Hovmöller diagrams (panels b, d and f) show how scaled anomalies in LAI, LST and SWE vary across different latitudes and over time. LAI anomalies (panel b) reveal strong seasonal dynamics and interannual variability, particularly in the middle latitudes, where positive anomalies were prominent in 2016 and in 2020. These shifts in vegetation activity may reflect climatic influences, such as warm winters, heatwaves or 190 droughts. LST anomalies (panel d) exhibit a consistent latitudinal pattern, featuring the warm winter of 2020 that coincides with SWE deficits in mid-latitude regions and SWE excess at high latitudes (panel f).



195 **Figure 2: New LC simulations over the whole European domain forced by ERA5 atmospheric variables from 2010 to 2022 at a spatial resolution of 0.25 degree x 0.25 degree: Mean values (a, c, e) and Hovmöller plot (b, d, f) of scaled anomalies (z-score) of (a, b) LAI, (c, d) LST, and (e, f) SWE.**



4.2 Assessment of New LC SWE simulations

Figure 3 shows the time series of the snow water equivalent (SWE) averaged over the entire European domain from 2010 to 2022. It compares the SWE derived from ESA CCI satellite data with the SWE simulated by Old LC and New LC, as well as the ERA5 SWE. All datasets capture the expected seasonal cycle of snow accumulation and melt, with consistent timing across years. However, the simulations consistently overestimate peak SWE values compared to the ESA CCI product, especially during the warm winter of 2020, when discrepancies between models and observations exceed 30 mm. Using New LC reduces the overestimation compared to the Old LC, narrowing the gap with the observations. ERA5 performs better in terms of amplitude and variability. However, some discrepancies remain with the satellite product, particularly during the warm winter of 2020.

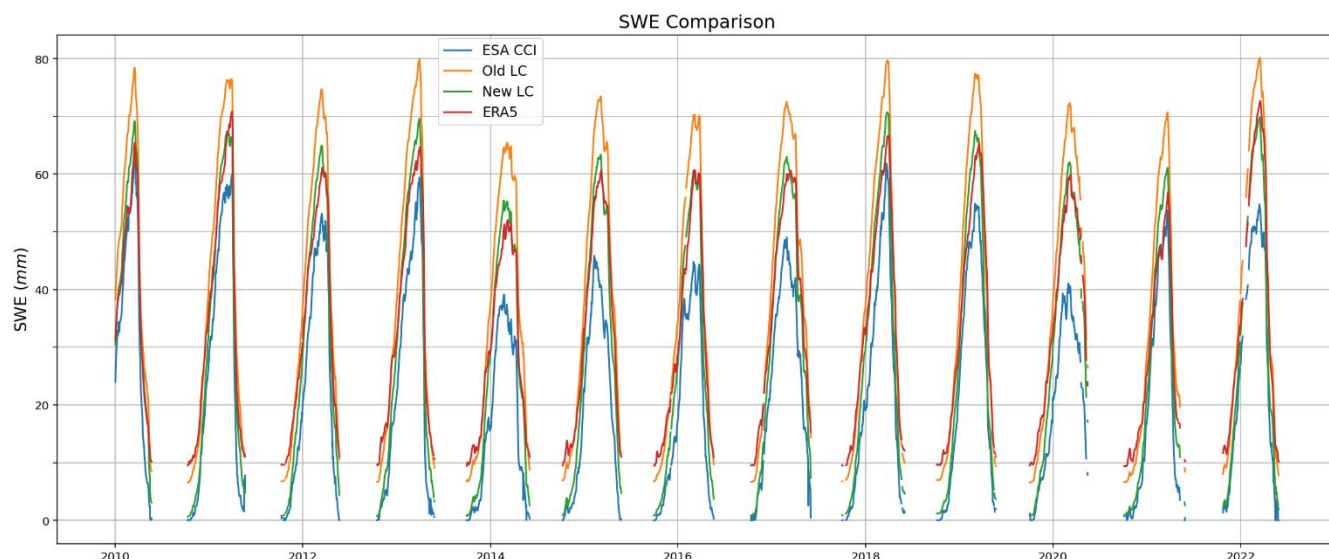


Figure 3: Time series of daily mean SWE values over the whole European domain from 2010 to 2022, based on the CCI SWE dataset, New LC, Old LC, and the ERA5 SWE.

210

Figure 4 presents the spatial patterns of SWE. The maps compare the mean SWE fields from CCI observations and New LC for the period 2010–2022, along with the difference between them. While the model generally captures the large-scale distribution of SWE, regional biases are evident, particularly in northern Europe. In regions like Sweden and Finland, the model underestimates SWE despite its tendency to overestimate peak values in the time series shown in Fig. 3.

215

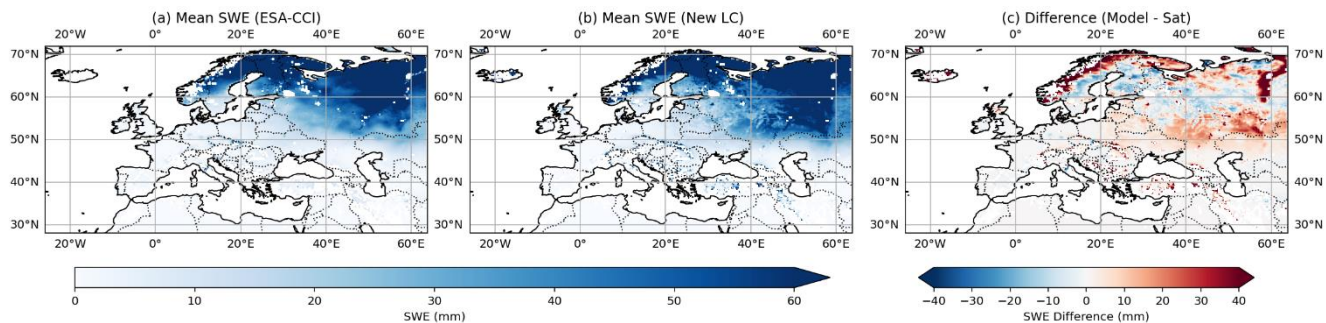


Figure 4: Maps of mean SWE values at altitudes below 1500 m across the whole of Europe from 2010 to 2022 derived from: (a) CCI SWE, (b) New LC, and (c) the difference between New LC and CCI SWE.

220 The statistical evaluation summarised in Table 1 provides further support for these findings. Using New LC results in a slight increase in the mean Pearson correlation coefficient between the modelled and observed SWE (from 0.70 to 0.71), indicating a marginal improvement in temporal agreement. While the mean ubRMSD remains unchanged at 16.9 mm, the overall RMSD is notably reduced from 29.2 mm to 23.3 mm. This reduction in RMSD is caused by the decrease in MB from 23.8 mm to 16.0 mm, suggesting that the improvement in alignment with the observed snow mass is the main cause of the
 225 reduction in RMSD. This suggests that the more detailed and updated land cover dataset better constrains snow accumulation processes in ISBA.

Table 1: Mean grid-cell level score values of the New LC and Old LC simulations for SWE and LST (both daytime and nighttime) over the 2010–2022 period. SWE score values are over the whole European domain. LST score values are for the westernmost part of the domain (10°W-30°E, 28.125°N-71.875°N). The number of observations and score values for ERA5 are also shown.

Model	vs. CCI variable	R	RMSD	ubRMSD	MB	Number
ERA5	SWE (mm)	0.73	18.1	14.6	10.7	83,962,378
Old LC		0.70	29.2	16.9	23.8	84,043,641
New LC		0.71	23.3	16.9	16.0	84,106,230
ERA5	Daytime LST (K)	0.96	4.8	4.4	- 1.8	18,056,129
Old LC		0.96	6.0	4.8	-3.6	19,311,176
New LC		0.96	6.1	4.9	- 3.7	19,311,164
ERA5	Nighttime LST (K)	0.97	3.0	2.5	1.6	23,109,907
Old LC		0.95	3.2	3.1	0.8	24,259,011
New LC		0.95	3.1	3.0	0.8	24,274,817

To further evaluate the impact of land cover representation on ISBA snow simulations, we move beyond domain-averaged statistics (see Table 1) and analyse the spatial distribution of performance score differences in relation to CCI SWE observations. Figure 5 shows the difference in performance between simulations using New LC and Old LC.

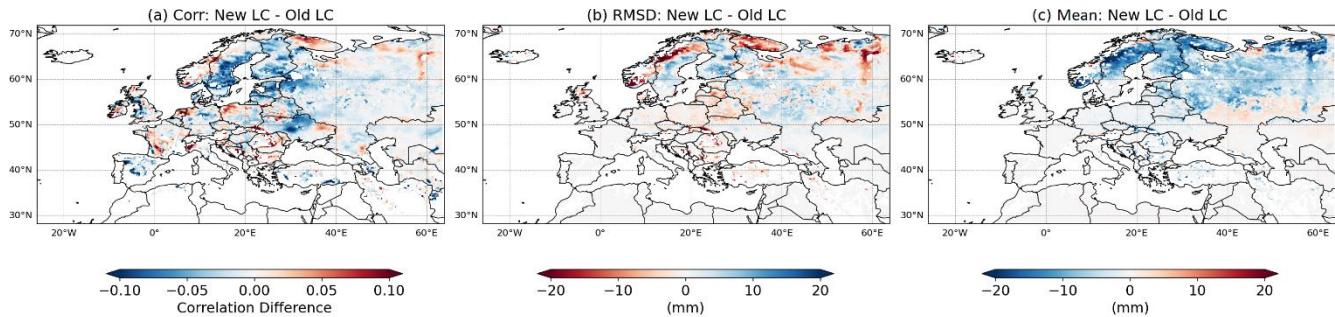


Figure 5: Spatial differences in the statistical performance metrics of New LC and Old LC SWE simulations with respect to CCI SWE observations over the whole European domain, over the 2010–2022 period: difference in (a) R , (b) RMSD and (c) mean difference of SWE between the two simulations. For R and RMSD, red zones indicate improvement (e.g. higher correlations or lower errors) when using New LC, while blue zones indicate degradation.

240

245

250

The comparison reveals a heterogeneous spatial response to changes in land cover. While improvements are evident in regions such as the Carpathians and parts of South-Eastern Europe, clear degradation is evident across large areas of northern Europe, particularly in Southern Sweden, and Finland. Conversely, reductions in the overestimation of SWE are observed in Northern Sweden and the Urals region.

Figure 6 illustrates the comparison between New LC SWE simulations and ERA5 SWE with respect to CCI SWE observations. The correlation difference map shows that, in general, ERA5 achieves a higher level of agreement with satellite-derived snow dynamics than the ISBA simulation, particularly across central and northern Europe. The RMSD difference map further highlights ERA5's superior performance across much of the domain, as indicated by the large areas of blue showing lower total errors. However, specific regions such as France and Northern Italy show local advantages for ISBA. The SWE difference map shows that New LC consistently produces higher mean SWE values than the ERA5 simulations across large areas, particularly in high-latitude and mountainous regions. These patterns align with the SWE biases in New LC (Fig. 4c), indicating that SWE positive biases are less pronounced in ERA5.

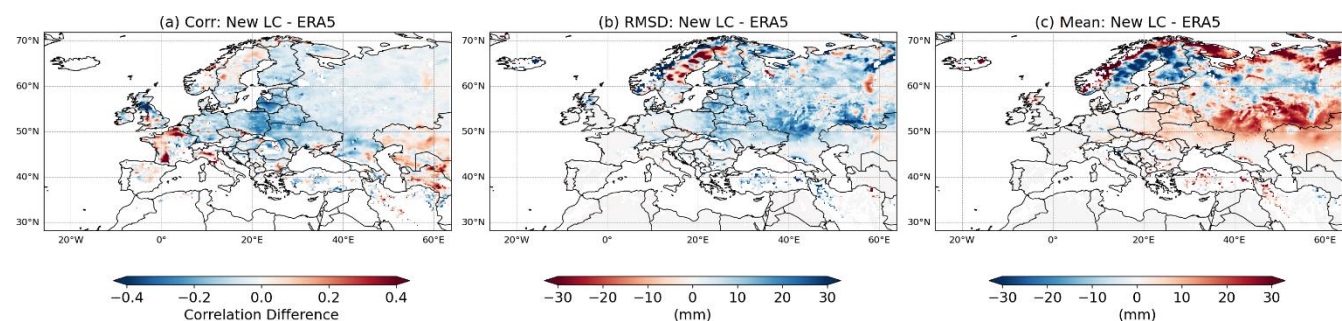
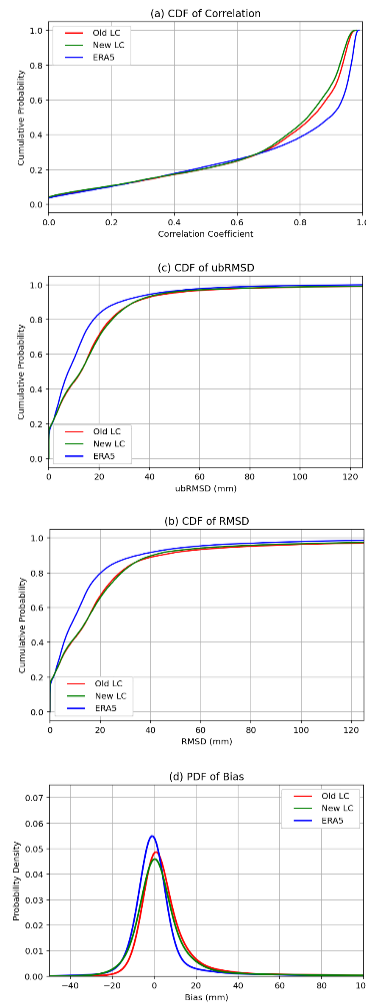


Figure 6: As in Fig. 5, except for differences between New LC and ERA5.

255



Figure 7 shows the cumulative distribution functions (CDFs) of score values to complement this spatial assessment, summarising model performance across all grid cells.



260

Figure 7: Cumulative distribution functions (CDFs) of (a) R , (b) RMSD, and (c) ubRMSD, alongside (d) the probability density function (PDF) of the bias, for SWE simulations from Old LC, New LC, and ERA5 (red, green, and blue, respectively), benchmarked against CCI SWE the whole European domain for the period 2010–2022.

265 Over half of the points have correlation values above 0.8, indicating that all three models (ERA5, Old LC and New LC) accurately depict the seasonal changes in snow water equivalent (SWE). Over 90% of the domain has RMSD values below 40 mm, indicating generally low errors in snow estimation. ERA5 displays the lowest RMSD and ubRMSD overall, with fewer instances of SWE overestimation. Although the bias spread of New LC is not reduced compared to the Old LC, instances of systematic overestimation are significantly reduced. Figure 7 also shows a slight improvement in the correlation
 270 CDF.



4.3 Assessment of ISBA LST simulations

Figure 9 shows that there is a persistent cold bias in ISBA daytime skin temperature over the westernmost part of the domain, while nighttime LST is slightly overestimated. As shown in Table 1, using New LC has a limited impact on the daytime and nighttime LST bias. It also shows that, while ERA5 LST is more consistent with observations than ISBA in terms of RMSD and ubRMSD, its nighttime warm bias is larger (1.6 K compared to 0.8 K for ISBA). ERA5 LST bias is reduced during the day compared with New LC (-1.8 K and -3.7 K, respectively).

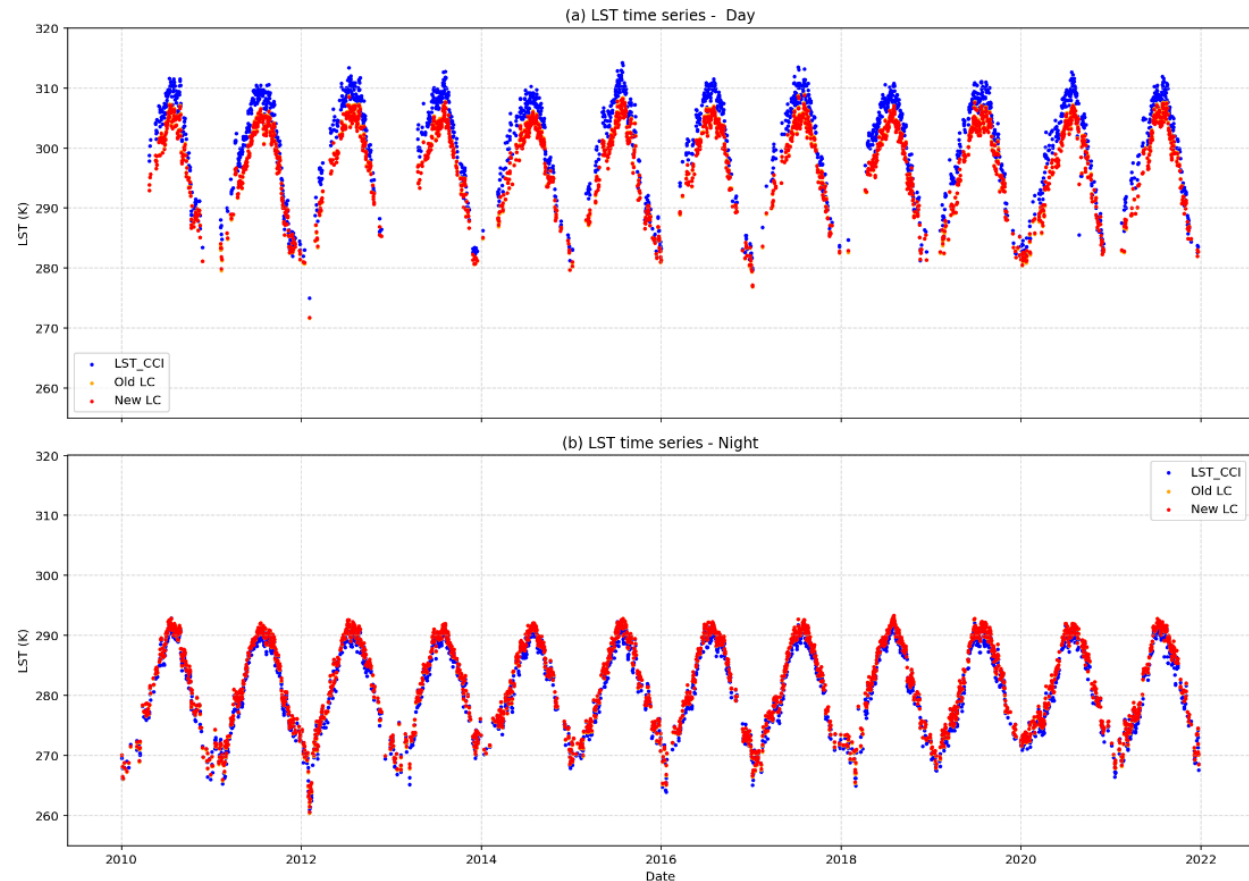


Figure 8: Time series of mean LST value over westernmost part of the domain (10°W-30°E, 28.125°N-71.875°N) from CCI LST, Old LC and New LC from 2010 to 2022: (a) daytime values at 13:30 LT for the observations, (b) nighttime at 01:30 LT, corresponding to ISBA simulations at 12:00 and 00:00 UTC, respectively.

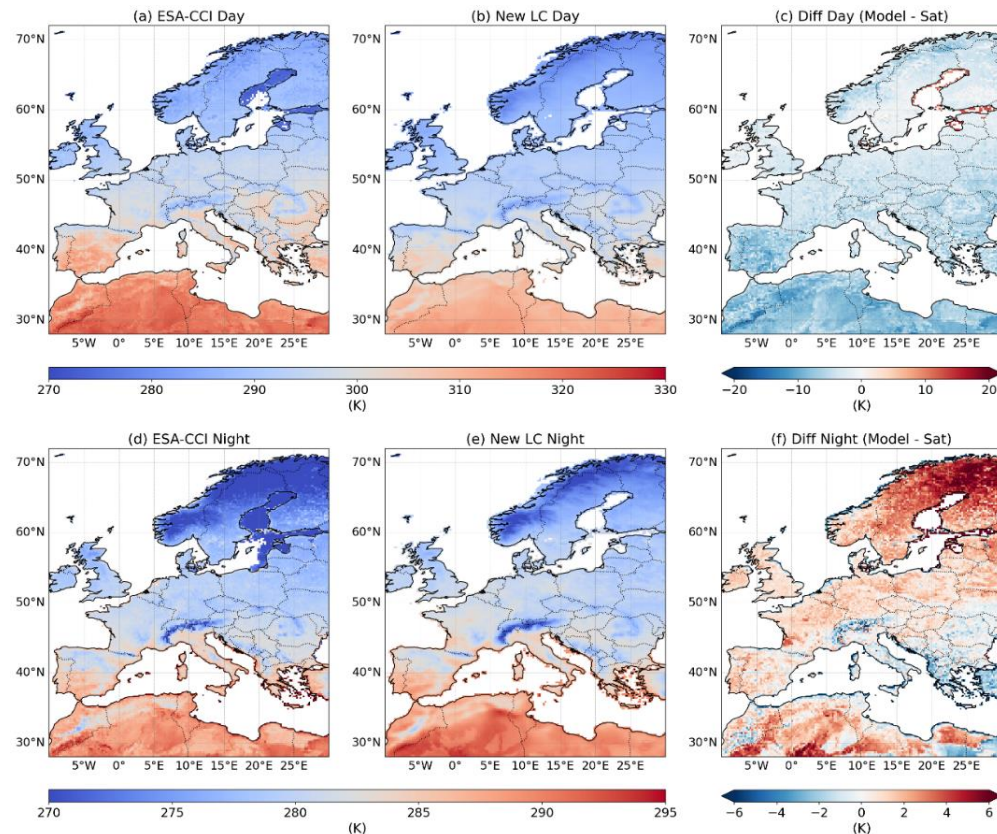
When considering only snow-free conditions (see Table S1), the LST score values are not fundamentally different to those shown in Table 1. When considering the December–January–February (DJF) winter season only (Table S2), the MB values are reduced, but the ubRMSD values of New LC increase. Considering snow-free conditions and the DJF season simultaneously (Table S3) yields smaller unRMSD values for New LC but not for ERA5.



5 Discussion

5.1 What causes the models' SWE bias?

As shown in Table 1 and Figure 3, both Old LC and New LC, as well as ERA5, tend to overestimate SWE with respect to the CCI SWE data. Using New LC reduces the mean SWE bias from 23.8 mm to 16.0 mm. As New LC has little impact on 290 the daytime cold bias or the nighttime warm bias, the overestimation of SWE cannot be explained by mean LST biases alone. Figure 9 shows the daytime and nighttime LST bias of New LC over the westernmost part of the domain.



295 **Figure 9: Maps showing the mean (a,b,c) daytime and (d,e,f) nighttime (bottom) LST values over westernmost part of the domain (10°W-30°E, 28.125°N-71.875°N), derived from (a, d) CCI LST, (b, e) New LC and (c, f) the difference between New LC and CCI LST.**

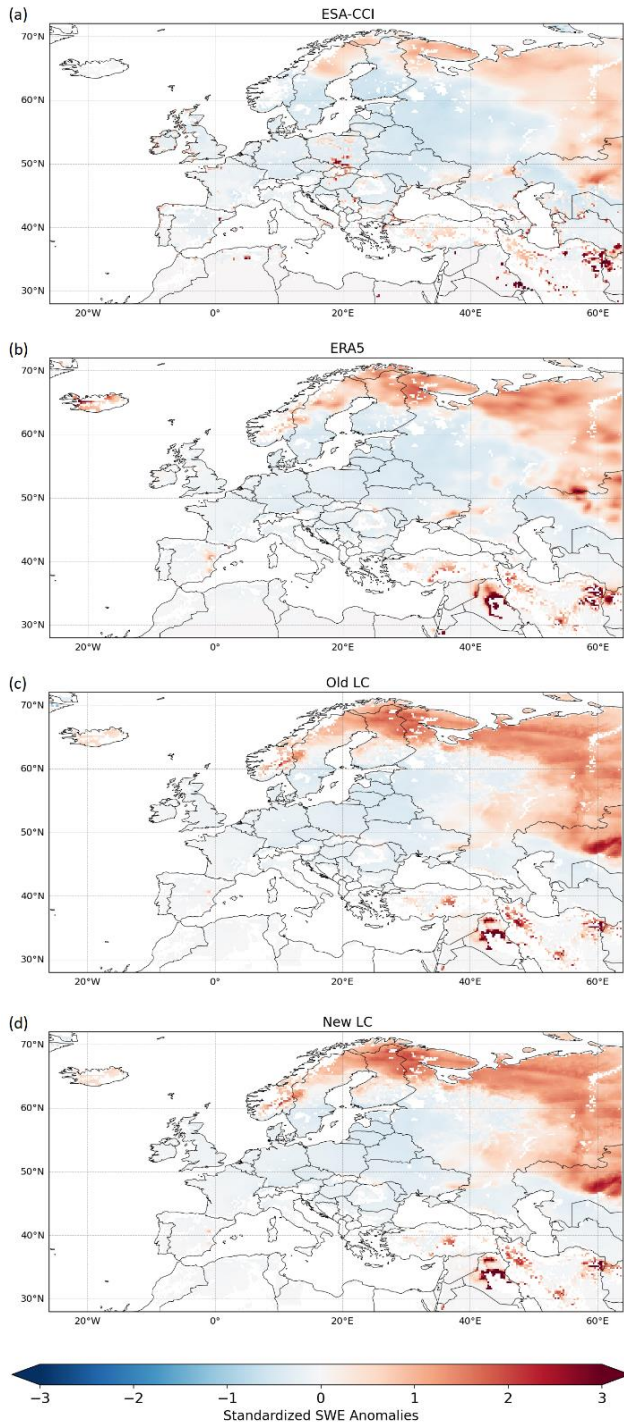
The cold bias in daytime LST is more pronounced in southern regions (North Africa and Spain) than in areas prone to snow. Conversely, the night-time warm bias is more pronounced in the north-eastern part of the domain, where snowfall is more 300 frequent. These results suggest that improving LC is beneficial for representing SWE, but this improvement cannot be explained by a better representation of LST. The limited response of daytime and nighttime LST to New LC can be attributed to the structural aspects of the ISBA model. This likely reflects the complex interplay of vegetation, turbulent



fluxes, solar radiation and soil heat storage. These factors go beyond static vegetation descriptors and cannot easily be corrected through land cover updates alone. New LC introduces a denser coniferous forest canopy in southern Sweden and 305 Finland than Old LC (see Fig. 1). Interactions between snow cover and forests are complex and can lead to increased model errors (Deschamps-Berger et al., 2025). New LC may also affect LAI throughout the seasons. The effect of using New LC on LAI simulations is presented in the supplementary material (Fig. S1). ERA5 also overestimates CCI SWE. Since ERA5 310 incorporates IMS snow observations, it is possible that the CCI SWE product itself may underestimate the actual SWE. A known limitation of the CCI SWE product is that the algorithm can only retrieve SWE data for snow packs with a thickness of less than 1 m. This is because the microwave brightness temperature signal saturates beyond a depth of 1 m or in the presence of wet snow (Barella et al., 2024).

5.2 Are the SWE estimates from the warm winter of 2020 consistent?

Figure 10 shows the scaled anomalies (z-score) of SWE for winter 2019-2020, which was a particularly warm winter season over Europe. All datasets reveal predominantly negative SWE anomalies across much of Europe, which is consistent with 315 the mild temperatures and reduced snow persistence reported for that winter in the mid-latitudes (Brown et al., 2020; Twardosz et al., 2021). Localised bands of positive anomalies appear in Russia, Kazakhstan, and Northern Scandinavia, which are likely to be associated with cold spells or above-average precipitation. The spatial patterns of the New LC and Old LC SWE anomalies show good agreement with the CCI SWE anomalies, particularly with regard to capturing the large-scale 320 negative anomaly across central and western Europe. However, the simulations tend to overestimate the extent and magnitude of positive anomalies in the northern and eastern regions. ERA5 successfully reproduces the broad anomaly structure, although it shows slightly more widespread positive anomalies in these regions. Conversely, the weaker positive anomalies of CCI SWE in these regions could suggest microwave signal saturation.



325 **Figure 10:** Scaled (z-score) anomalies of SWE for winter 2020, relative to the 2010–2022 climatology: (a) CCI SWE, (b) ERA5
SWE, (c) Old LC SWE, and (d) New LC SWE. Red colours indicate positive anomalies (i.e. more snow than the climatological
mean), and blue colours indicate negative anomalies (i.e. a snow deficit).



6 Conclusion

This study assessed the impact of incorporating the ECOCLIMAP-SG land cover dataset (derived from the ESA CCI land cover) into the SURFEX version 9 ISBA land surface model across Europe between 2010 and 2022. The focus was on the simulation performance of snow water equivalent (SWE). Benchmarking against ESA CCI SWE and ERA5 revealed that the updated land cover improved the ISBA model's performance, reducing the root mean square deviation (RMSD) by around 8 mm and marginally enhancing the correlation. Spatial analyses demonstrate that ECOCLIMAP-SG notably enhances SWE simulation in central and south-eastern Europe. Conversely, performance deteriorated in certain forested regions in the north, likely due to altered snow–vegetation interactions. ERA5 remains the best-performing dataset in terms of absolute error, but ISBA with ECOCLIMAP-SG more accurately captures the spatial variability of snow accumulation. Beyond SWE, our analysis of land surface temperature (LST) revealed potential model biases that could affect snow simulations. Specifically, ISBA shows cold and warm biases during the daytime and nighttime, respectively, compared to ESA CCI LST. However, these biases alone cannot fully account for the overestimation of SWE. It is possible that the CCI SWE product itself underestimates the actual SWE.

340

Code availability. SURFEX can be downloaded freely at https://www.umr-cnrm.fr/surfex/data/OPEN-SURFEX/open_surfex_v9_0_0_20231024.tar.gz (last access: January 2026; CNRM, 2023). It is provided under a CECILL-C License (French equivalent to the L-GPL licence).

345

Data availability. ESA Land Cover Climate Change Initiative (Land_Cover_cci) Global Land Cover Maps, Version 2.0.7, are available from <https://catalogue.ceda.ac.uk/uuid/b382ebe6679d44b8b0e68ea4ef4b701c> (last access: January 2026), CCI global Aqua MODIS LST data (version 4) are available from https://gws-access.jasmin.ac.uk/public/esacci_lst/AQUA_MODIS_L3C_0.01/4.00/ (last access: January 2026) (<https://doi.org/10.5285/d56a6215ce394ddd8dff6bea5dbb0780>), CCI global SWE data (version 3.1) are available from <https://catalogue.ceda.ac.uk/uuid/9d9bfc488ec54b1297eca2c9662f9c81/> (last access: January 2026), ERA5 global SWE data are available from the C3S Climate Data Store <https://cds.climate.copernicus.eu/datasets/reanalysis-era5-single-levels?tab=download> (last access: January 2026).

355

Supplement. The supplement related to this article is available online at:



360 *Author contributions.* The experiments were designed by ORM, BB and JCC. CA, DT, DG and CL provided recommendations on how to use the benchmarking datasets. ORM and BB performed the SURFEX version 9 simulations. ORM wrote the paper. All co-authors participated in analysing the results and revising the paper.

365 *Competing interests.* The contact author has declared that none of the authors has any competing interests.

370

Disclaimer. Publisher's note: Copernicus Publications remains neutral with regard to jurisdictional claims made in the text, published maps, institutional affiliations, or any other geographical representation in this paper. While Copernicus Publications makes every effort to include appropriate place names, the final responsibility lies with the authors. Views and opinions expressed are however those of the author(s) only and do not necessarily reflect those of the European Union or the Commission. Neither the European Union nor the granting authority can be held responsible for them.

375 *Acknowledgements.* The authors would like to thank the ESA's Climate Change Initiative (CCI) Land Cover, Land Surface Temperature (LST) and Snow projects for providing benchmarking data, and the Copernicus Climate Change Service for providing ERA5 data.

380 *Financial support.* This research has been supported by the European Space Agency (ESA Climate Change Initiative Climate Model User Group (ESA CCI CMUG)) and by the Copernicus Climate Change Service Evolution (CERISE) project. The CERISE project (grant agreement No101082139) is funded by the European Union. Views and opinions expressed are however those of the author(s) only and do not necessarily reflect those of the European Union or the Commission. Neither the European Union nor the granting authority can be held responsible for them.

385



References

Barella, R., Mortimer, C., Marin, C., Schwaizer, G., Mölg, N., Nagler, T., Wunderle, S., Xiao, X., Luoju, K., Venäläinen, P., Takala, M., Pulliainen, J., Lemmetyinen, J., Moisander, M., and Solberg, R.: ESA CCI+ Snow ECV: Product User Guide, version 4.0, April 2024, http://snow-cci.enveo.at/documents/Snow_cci_D4.3_PUG_v4.0.pdf (last access: January 390 2026), 2024.

Barella-Ortiz, A., Quintana-Seguí, P., Dari, J., Brocca, L., Altés, V., Villar, J. M., Paolini, G., José Escorihuela, M., Bonan, B., Calvet, J.-C., and Tzanos, D.: Improved SAFRAN forcing and ECOCLIMAP-SG datasets to simulate irrigation over the Ebro basin, EGU General Assembly Conference Abstracts, ADS Bibcode: 2022EGUGA..24.7834B, EGU22-7834, <https://doi.org/10.5194/egusphere-egu22-7834>, 2022.

395 Bélair, S., Crevier, L.-P., Mailhot, J., Bilodeau, B., and Delage, Y.: Operational Implementation of the ISBA Land Surface Scheme in the Canadian Regional Weather Forecast Model. Part I: Warm Season Results, Journal of Hydrometeorology, 4, 352–370, [https://doi.org/10.1175/1525-7541\(2003\)4<352:OITOL>2.0.CO;2](https://doi.org/10.1175/1525-7541(2003)4<352:OITOL>2.0.CO;2), 2003a.

Bélair, S., Brown, R., Mailhot, J., Bilodeau, B., and Crevier, L.-P.: Operational Implementation of the ISBA Land Surface Scheme in the Canadian Regional Weather Forecast Model. Part II: Cold Season Results, Journal of Hydrometeorology, 4, 400 371–386, [https://doi.org/10.1175/1525-7541\(2003\)4<371:OITOL>2.0.CO;2](https://doi.org/10.1175/1525-7541(2003)4<371:OITOL>2.0.CO;2), 2003b.

Blyth, E. M., Arora, V. K., Clark, D. B., Dadson, S. J., De Kauwe, M. G., Lawrence, D. M., Melton, J. R., Pongratz, J., Turton, R. H., Yoshimura, K., and Yuan, H.: Advances in Land Surface Modelling, Curr Clim Change Rep, 7, 45–71, <https://doi.org/10.1007/s40641-021-00171-5>, 2021.

405 Boone, A. and Etchevers, P.: An Intercomparison of Three Snow Schemes of Varying Complexity Coupled to the Same Land Surface Model: Local-Scale Evaluation at an Alpine Site, J. Hydrometeor., 2, 374–394, [https://doi.org/10.1175/1525-7541\(2001\)002<0374:AIOTSS>2.0.CO;2](https://doi.org/10.1175/1525-7541(2001)002<0374:AIOTSS>2.0.CO;2), 2001.

Boone, A., Masson, V., Meyers, T., and Noilhan, J.: The Influence of the Inclusion of Soil Freezing on Simulations by a Soil–Vegetation–Atmosphere Transfer Scheme, J. Appl. Meteor., 39, 1544–1569, [https://doi.org/10.1175/1520-0450\(2000\)039<1544:TIOTIO>2.0.CO;2](https://doi.org/10.1175/1520-0450(2000)039<1544:TIOTIO>2.0.CO;2), 2000.

410 Bounoua, L., DeFries, R., Collatz, G. J., Sellers, P., and Khan, H.: Effects of Land Cover Conversion on Surface Climate, Climatic Change, 52, 29–64, <https://doi.org/10.1023/A:1013051420309>, 2002.

Brown, R., de Rosnay, P., Robinson, D., and Luoju, K.: Snow Assessments: Northern Hemisphere 2019–2020 Winter Snow Cover, WMO Global Cryosphere Watch, <https://globalcryospherewatch.org/snow-assessments-2020> (last access: January 2026), 2020.

415 Calvet, J.-C. and Champeaux, J.-L.: L'apport de la télédétection spatiale à la modélisation des surfaces continentales, La Météorologie, 2020, 52–58, <https://doi.org/10.37053/lameteorologie-2020-0016>, 2020.



Calvet, J.-C., Noilhan, J., Roujean, J.-L., Bessemoulin, P., Cabelguen, M., Olioso, A., and Wigneron, J.-P.: An interactive vegetation SVAT model tested against data from six contrasting sites, *Agricultural and Forest Meteorology*, 92, 73–95, [https://doi.org/10.1016/S0168-1923\(98\)00091-4](https://doi.org/10.1016/S0168-1923(98)00091-4), 1998.

420 Calvet, J.-C., Gibelin, A.-L., Roujean, J.-L., Martin, E., Le Moigne, P., Douville, H., and Noilhan, J.: Past and future scenarios of the effect of carbon dioxide on plant growth and transpiration for three vegetation types of southwestern France, *Atmospheric Chemistry and Physics*, 8, 397–406, <https://doi.org/10.5194/acp-8-397-2008>, 2008.

Chiu, J., Paredes-Mesa, S., Lakhankar, T., Romanov, P., Krakauer, N., Khanbilvardi, R., and Ferraro, R.: Intercomparison and Validation of MIRS, MSPPS, and IMS Snow Cover Products, *Adv. Meteorol.*, 2020, 4532478, <https://doi.org/10.1155/2020/4532478>, 2020.

425 CNRM: SURFEX code, CNRM, https://www.umr-cnrm.fr/surfex/data/OPEN-SURFEX/open_surfex_v9_0_0_20231024.tar.gz (last access: January 2026), 2023.

Crow, W. T., Kumar, S. V., and Bolten, J. D.: On the utility of land surface models for agricultural drought monitoring, *Hydrology and Earth System Sciences*, 16, 3451–3460, <https://doi.org/10.5194/hess-16-3451-2012>, 2012.

430 Decharme, B., Delire, C., Minvielle, M., Colin, J., Vergnes, J.-P., Alias, A., et al.: Recent changes in the ISBA-CTRP land surface system for use in the CNRM-CM6 climate model and in global off-line hydrological applications. *Journal of Advances in Modeling Earth Systems*, 11, 1207–1252, <https://doi.org/10.1029/2018MS001545>, 2019.

Decharme, B., Brun, E., Boone, A., Delire, C., Le Moigne, P., and Morin, S.: Impacts of snow and organic soils parameterization on northern Eurasian soil temperature profiles simulated by the ISBA land surface model, *The Cryosphere*, 10, 853–877, <https://doi.org/10.5194/tc-10-853-2016>, 2016.

435 Delire, C., Séférian R., Decharme B., Alkama R., Calvet J.-C., Carrer D., Gibelin A.-L., Joetzjer E., Morel X., Rocher M., and Tzanos, D.: The global land carbon cycle simulated with ISBA-CTRP: improvements over the last decade, *J. Adv. Model. Earth Sy.*, 12, e2019MS001886, <https://doi.org/10.1029/2019MS001886>, 2020.

Deschamps-Berger, C., López-Moreno, J. I., Gascoin, S., Mazzotti, G., and Boone, A.: Where snow and forest meet: A 440 global atlas, *Geophysical Research Letters*, 52, e2024GL113684, <https://doi.org/10.1029/2024GL113684>, 2025.

Druel, A., Munier, S., Mucia, A., Albergel, C., and Calvet, J.-C.: Implementation of a new crop phenology and irrigation scheme in the ISBA land surface model using SURFEX_v8.1, *Geosci. Model Dev.*, 15, 8453–8471, <https://doi.org/10.5194/gmd-15-8453-2022>, 2022.

445 Etchanchu, J., Rivalland, V., Gascoin, S., Cros, J., Tallec, T., Brut, A., and Boulet, G.: Effects of high spatial and temporal resolution Earth observations on simulated hydrometeorological variables in a cropland (southwestern France), *Hydrology and Earth System Sciences*, 21, 5693–5708, <https://doi.org/10.5194/hess-21-5693-2017>, 2017.

Faroux, S., Kaptué Tchuenté, A. T., Roujean, J.-L., Masson, V., Martin, E., and Le Moigne, P.: ECOCLIMAP-II/Europe: a twofold database of ecosystems and surface parameters at 1 km resolution based on satellite information for use in land surface, meteorological and climate models, *Geoscientific Model Development*, 6, 563–582, <https://doi.org/10.5194/gmd-6-563-2013>, 2013.



Gao, C., Jiang, X., Qian, Y., Qiu, S., Ma, L., and Li, Z.: A neural network based method for land surface temperature retrieval from AMSR-E passive microwave data, in: 2013 IEEE International Geoscience and Remote Sensing Symposium - IGARSS, 2013 IEEE International Geoscience and Remote Sensing Symposium - IGARSS, 469–472, <https://doi.org/10.1109/IGARSS.2013.6721194>, 2013.

455 Ghent, D. J., Corlett, G. K., Göttsche, F. -M., and Remedios, J. J.: Global Land Surface Temperature From the Along-Track Scanning Radiometers, *JGR Atmospheres*, 122, <https://doi.org/10.1002/2017JD027161>, 2017.

Giard, D., and Bazile, E.: Implementation of a New Assimilation Scheme for Soil and Surface Variables in a Global NWP Model, *Mon. Weather Rev.*, 128, 997–1015, [https://doi.org/10.1175/1520-0493\(2000\)128<0997:IOANAS>2.0.CO;2](https://doi.org/10.1175/1520-0493(2000)128<0997:IOANAS>2.0.CO;2), 2000.

460 Hersbach, H., Bell, B., Berrisford, P., Hirahara, S., Horányi, A., Muñoz-Sabater, J., Nicolas, J., Peubey, C., Radu, R., Schepers, D., Simmons, A., Soci, C., Abdalla, S., Abellán, X., Balsamo, G., Bechtold, P., Biavati, G., Bidlot, J., Bonavita, M., De Chiara, G., Dahlgren, P., Dee, D., Diamantakis, M., Dragani, R., Flemming, J., Forbes, R., Fuentes, M., Geer, A., Haimberger, L., Healy, S., Hogan, R. J., Hólm, E., Janisková, M., Keeley, S., Laloyaux, P., Lopez, P., Lupu, C., Radnoti, G., de Rosnay, P., Rozum, I., Vamborg, F., Villaume, S., and Thépaut, J.-N.: The ERA5 global reanalysis, *Quarterly Journal of the Royal Meteorological Society*, 146, 1999–2049, <https://doi.org/10.1002/qj.3803>, 2020.

465 de Jeu, R. A. M., Wagner, W., Holmes, T. R. H., Dolman, A. J., van de Giesen, N. C., and Friesen, J.: Global Soil Moisture Patterns Observed by Space Borne Microwave Radiometers and Scatterometers, *Surv Geophys*, 29, 399–420, <https://doi.org/10.1007/s10712-008-9044-0>, 2008.

Jimenez, C. and Prigent, C.: ESA Land Surface Temperature Climate Change Initiative (LST_cci): All-weather MicroWave 470 Land Surface Temperature (MW-LST) global data record (1996-2020), <https://doi.org/10.5285/058D3AD17A084F0BB8DC9B5DC5EFDB7F>, 2022.

Jose, V., Chandrasekar, A., and Reddy Rodda, S.: Impact of Historical Land Cover Changes on Land Surface Characteristics over the Indian Region Using Land Information System, *Pure Appl. Geophys.*, 181, 2561–2588, <https://doi.org/10.1007/s00024-024-03523-y>, 2024.

475 Kaptue, A., Roujean, J.-L., and Faroux, S.: ECOCLIMAP-II programme: A new land cover classification at 1 km from MODIS and vegetation data time series over the western Africa in the frame of AMMA project, in: 2009 IEEE International Geoscience and Remote Sensing Symposium, 2009 IEEE International Geoscience and Remote Sensing Symposium, IV-1023-IV–1026, <https://doi.org/10.1109/IGARSS.2009.5417555>, 2009.

Kouki, K., Luojus, K., and Riihelä, A.: Evaluation of snow cover properties in ERA5 and ERA5-Land with several satellite-based datasets in the Northern Hemisphere in spring 1982–2018, *The Cryosphere*, 17, 5007–5026, <https://doi.org/10.5194/tc-17-5007-2023>, 2023.

480 Lawrence, P. J. and Chase, T. N.: Representing a new MODIS consistent land surface in the Community Land Model (CLM 3.0), *Journal of Geophysical Research (Biogeosciences)*, 112, G01023, <https://doi.org/10.1029/2006JG000168>, 2007.



Levis, S.: Modeling vegetation and land use in models of the Earth System, *WIREs Climate Change*, 1, 840–856, 485 <https://doi.org/10.1002/wcc.83>, 2010.

Li, W., MacBean, N., Ciais, P., Defourny, P., Lamarche, C., Bontemps, S., Houghton, R. A., and Peng, S.: Gross and net land cover changes in the main plant functional types derived from the annual ESA CCI land cover maps (1992–2015), *Earth System Science Data*, 10, 219–234, <https://doi.org/10.5194/essd-10-219-2018>, 2018.

Ling, X., Huang, Y., Guo, W., Wang, Y., Chen, C., Qiu, B., Ge, J., Qin, K., Xue, Y., and Peng, J.: Comprehensive evaluation of satellite-based and reanalysis soil moisture products using in situ observations over China, *Hydrology and Earth System Sciences*, 25, 4209–4229, <https://doi.org/10.5194/hess-25-4209-2021>, 2021.

Liu, E., Zhu, Y., Lü, H., Bonan, B., Munier, S., and Calvet, J.-C.: Impact of leaf area index assimilation and gauge-corrected precipitation on land surface variables in LDAS-Monde: a case study over China, *J. Hydrol.*, 133304, <https://doi.org/10.1016/j.jhydrol.2025.133304>, 2025.

495 Liu, S., Liu, X., Yu, L., Wang, Y., Zhang, G. J., Gong, P., Huang, W., Wang, B., Yang, M., and Cheng, Y.: Climate response to introduction of the ESA CCI land cover data to the NCAR CESM, *Clim Dyn*, 56, 4109–4127, <https://doi.org/10.1007/s00382-021-05690-3>, 2021.

Luojas, K., Pulliainen, J., Takala, M., Lemmetyinen, J., Mortimer, C., Derksen, C., Mudryk, L., Moisander, M., Hiltunen, M., Smolander, T., Ikonen, J., Cohen, J., Salminen, M., Norberg, J., Veijola, K., Venäläinen, P.: GlobSnow v3.0 Northern 500 Hemisphere snow water equivalent dataset, *Sci Data* 8, 163, <https://doi.org/10.1038/s41597-021-00939-2>, 2021.

Luojas, K., Venäläinen, P., Moisander, M., Pulliainen, J., Takala, M., Lemmetyinen, J., Derksen, C., Mortimer, C., Mudryk, L., Schwaizer, G., and Nagler, T.: ESA Snow Climate Change Initiative (Snow_cci): Snow Water Equivalent (SWE) level 3C daily global climate research data package (CRDP) (1979 - 2022), version 3.1 [data set], <https://doi.org/10.5285/9D9BFC488EC54B1297ECA2C9662F9C81>, 2024.

505 Maas, A. E., Rottensteiner, F., Alobeid, A., and Heipke, C.: Multitemporal Classification Under Label Noise Based on Outdated Maps, *Photogrammetric Engineering & Remote Sensing*, 84, 263–277, <https://doi.org/10.14358/PERS.84.5.263>, 2018.

Masson, V., Le Moigne, P., Martin, E., Faroux, S., Alias, A., Alkama, R., Belamari, S., Barbu, A., Boone, A., Bouyssel, F., Brousseau, P., Brun, E., Calvet, J.-C., Carrer, D., Decharme, B., Delire, C., Donier, S., Essaouini, K., Gibelin, A.-L., 510 Giordani, H., Habets, F., Jidane, M., Kerdraon, G., Kourzeneva, E., Lafaysse, M., Lafont, S., Lebeaupin Brossier, C., Lemonsu, A., Mahfouf, J.-F., Marguinaud, P., Mokhtari, M., Morin, S., Pigeon, G., Salgado, R., Seity, Y., Taillefer, F., Tanguy, G., Tulet, P., Vincendon, B., Vionnet, V., and Volodire, A.: The SURFEXv7.2 land and ocean surface platform for coupled or offline simulation of Earth surface variables and fluxes, *Geosci. Model Dev.*, 6, 929–960, <https://doi.org/10.5194/gmd-6-929-2013>, 2013.

515 Mishra, A. K., Dinesh, A. S., Kumari, A., and Pandey, L. K.: Precipitation Extremes over India in a Coupled Land–Atmosphere Regional Climate Model: Influence of the Land Surface Model and Domain Extent, *Atmosphere*, 15, 44, <https://doi.org/10.3390/atmos15010044>, 2024.



520 Muñoz-Sabater, J., Dutra, E., Agustí-Panareda, A., Albergel, C., Arduini, G., Balsamo, G., Boussetta, S., Choulga, M., Harrigan, S., Hersbach, H., Martens, B., Miralles, D. G., Piles, M., Rodríguez-Fernández, N. J., Zsoter, E., Buontempo, C., and Thépaut, J.-N.: ERA5-Land: a state-of-the-art global reanalysis dataset for land applications, *Earth System Science Data*, 13, 4349–4383, <https://doi.org/10.5194/essd-13-4349-2021>, 2021.

525 Orsolini, Y., Wegmann, M., Dutra, E., Liu, B., Balsamo, G., Yang, K., de Rosnay, P., Zhu, C., Wang, W., Senan, R., and Arduini, G.: Evaluation of snow depth and snow cover over the Tibetan Plateau in global reanalyses using in situ and satellite remote sensing observations, *The Cryosphere*, 13, 2221–2239, <https://doi.org/10.5194/tc-13-2221-2019>, 2019.

530 Pérez-Planells, L., Ghent, D., Ermida, S., Martin, M., and Götsche, F.-M.: Retrieval Consistency between LST CCI Satellite Data Products over Europe and Africa, *Remote Sensing*, 15, 3281, <https://doi.org/10.3390/rs15133281>, 2023.

Quintana-Seguí, P., Barella-Ortiz, A., Regueiro-Sanfiz, S., and Miguez-Macho, G.: The Utility of Land-Surface Model Simulations to Provide Drought Information in a Water Management Context Using Global and Local Forcing Datasets, *Water Resour Manage*, 34, 2135–2156, <https://doi.org/10.1007/s11269-018-2160-9>, 2020.

535 Raoult, N., Delorme, B., Bastrikov, V., Ottlé, C., and Peylin, P.: Global Comparison of Surface Soil Moisture from the ESA CCI Combined Product and the Orchidee Land-Surface Model, in: IGARSS 2018 - 2018 IEEE International Geoscience and Remote Sensing Symposium, IGARSS 2018 - 2018 IEEE International Geoscience and Remote Sensing Symposium, 3711–3714, <https://doi.org/10.1109/IGARSS.2018.8517696>, 2018.

540 Reiners, P., Asam, S., Frey, C., Holzwarth, S., Bachmann, M., Sobrino, J., Götsche, F.-M., Bendix, J., and Kuenzer, C.: Validation of AVHRR Land Surface Temperature with MODIS and In Situ LST—A TIMELINE Thematic Processor, *Remote Sensing*, 13, 3473, <https://doi.org/10.3390/rs13173473>, 2021.

Rojas Muñoz, O. J., Chiriaco, M., Bastin, S., and Ringard, J.: Estimation of the terms acting on local $1\text{ }h$ surface temperature variations in Paris region: the specific contribution of clouds, *Atmospheric Chemistry and Physics*, 21, 15699–15723, <https://doi.org/10.5194/acp-21-15699-2021>, 2021.

545 Saeedi, M., Sharafati, A., and Tavakol, A.: Evaluation of gridded soil moisture products over varied land covers, climates, and soil textures using in situ measurements: A case study of Lake Urmia Basin, *Theor Appl Climatol*, 145, 1053–1074, <https://doi.org/10.1007/s00704-021-03678-x>, 2021.

Seo, E. and Dirmeyer, P. A.: Improving the ESA CCI Daily Soil Moisture Time Series with Physically Based Land Surface Model Datasets Using a Fourier Time-Filtering Method, *Journal of Hydrometeorology*, 23, 473–489, <https://doi.org/10.1175/JHM-D-21-0120.1>, 2022.

550 Sun, H., Y. Fang, S.A. Margulis, C. Mortimer, L. Mudryk, and C. Derksen: Evaluation of the Snow Climate Change Initiative (Snow CCI) snow-covered area product within a mountain snow water equivalent reanalysis, *The Cryosphere*, 2025, 19, 2017–2036, <https://doi.org/10.5194/tc-19-2017-2025>, 2025.

Twardosz, R., Walanus, A., and Guzik, I.: Warming in Europe: Recent Trends in Annual and Seasonal temperatures, *Pure Appl. Geophys.*, 178, 4021–4032, <https://doi.org/10.1007/s00024-021-02860-6>, 2021.



Wang, L., Arora, V. K., Bartlett, P., Chan, E., and Curasi, S. R.: Mapping of ESA's Climate Change Initiative land cover data to plant functional types for use in the CLASSIC land model, *Biogeosciences*, 20, 2265–2282, <https://doi.org/10.5194/bg-20-2265-2023>, 2023.